The 5th International Symposium - Supercritical CO2 Power Cycles – Paper #51
March 28 to 31, 2016 San Antonio, Texas

PARAMETRIC ANALYSIS OF SCO_2 POWER CYCLES OPERATING AT MODERATE TEMPERATURES

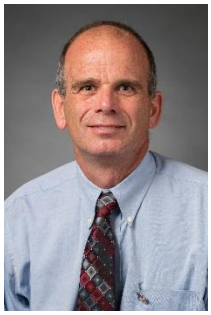

Peter D. Friedman, PhD, PE
Newport News Shipbuilding, a Division of
Huntington Ingalls Industries
Peter.D.Friedman@HII-NNS.com

Michael P. Rapp
Newport News Shipbuilding, a Division of
Huntington Ingalls Industries
MP.Rapp@HII-NNS.com

Abstract

A parametric analysis of a recuperated sCO_2 power cycle operating at moderate temperatures was conducted using Engineering Equation Solver from F-Chart® Software (EES). The results indicate that subcritical cycles and critical cycles demonstrate large changes in efficiency for slight variations in compressor suction pressure. For example, a cycle with its compressor suction temperature equal to the critical temperature demonstrates a maximum thermal efficiency when its compressor suction pressure is slightly greater than the critical pressure. When pressure is reduced from this optimum, thermal efficiency drops rapidly (about a 25% reduction for a 2% change in pressure); whereas when pressure is increased, efficiency drops gradually. For compressor suction temperatures less than the critical temperature, efficiency undergoes a step change reduction for pressures less than saturation and a gradual reduction as pressure is increased. This step change can drop efficiency by more than 75%. Compressor suction temperatures greater than the critical temperature results in a maximum that decreases smoothly as pressure is either increased or decreased from the optimal. Parametric analysis reveals the peak efficiency varies from about 29% to 19% as compressor suction temperature increases from 90% to 110% of the critical temperature under the operating condition modeled. Further parametric analyses demonstrate an increase in efficiency with cycle high temperatures, and reductions with increasing pressure drops, decreasing component efficiencies and decreasing recuperator effectiveness.

Nomenclature:

A	Area
C	Flow heat capacity $\left(\dot{m}c_P\right)$
c_p	Specific heat
D	Pipe diameter
f	Moody friction factor
h	Enthalpy, convective heat transfer coefficient
i	Irreversibility or exergy destruction per unit mass
k	Fluid thermal conductivity
K	Piping component head loss coefficient
ke	Specific kinetic energy ($V^2/2$, where V represents velocity)
L	Length
$\dot{m}$	Mass flow rate
Nu	Nusselt number $\left(hD/k\right)$
P , $P*$	Pressure, Pressure normalized by critical pressure
pe	Specific potential energy (gz , where z represents elevation)
Pr	Prandtl number of the fluid
q	Specific heat flow
$\dot{Q}$	Rate of heat transfer
q_{Max}	The rate heat transfer that would occur in an infinitely long counterflow heat exchanger
R	Heat transfer resistance
Re	Reynolds number
S	Entropy
S_{Gen}	Entropy generated in a process
T , $T*$	Temperature, Temperature normalized by critical temperature
V	Velocity
W	Specific work
ΔP	Flow pressure drop
ε	Recuperator Effectiveness, Piping system absolute roughness
ϕ	Closed system exergy
η	Efficiency
ρ	Density
ψ	Flow exergy

Subscripts

0	Dead state property (used in $h_{o,}P_o,T_o,s_o$)
$1,2$	Component inlet and outlet, respectively
C,T	Compressor and turbine, respectively
C,H	Cold and hot fluids, respectively
Th	Thermal efficiency (refers to energy transformations within the working fluid)
R,S	Heat rejected and supplied, respectively

S	The state point that would be reached in an isentropic process
I, II	First law (or energy) and second law or exergy) basis, respectively

I. Introduction

Since the concept was first introduced by Sulzer [11], supercritical CO_2, operating in a closed loop modified Brayton/Rankine cycle, has offered great promise as a result of its availability, high density, benign nature, wide temperature range and high thermal capacity [5]. Its energy density allows the use of smaller and simpler turbomachinery, and it eliminates a number of support systems when compared to traditional steam cycles. Additionally, CO_2 power cycles can operate efficiently over a much wider temperature range than steam cycles, organic Rankine cycle (ORC) systems and air bottoming cycles [5].

Although, in comparison to steam, efficiency improvements are only achieved at elevated temperatures, in cases where physical space is at a premium, such as naval vessels, sCO_2 cycles may still be advantageous, even under moderate temperature conditions. The potential higher density thermal to mechanical energy conversion has the potential to free up space enabling electric drive systems, and smaller components allow for greater installed redundancy. Additionally, components of electrically driven ships have much greater flexibility in placement, and the single phase working fluid in sCO_2 plants also improves placement flexibility and reduces manning requirements.

In this study, we model a recuperated sCO_2 power cycle operating at moderate temperatures using Engineering Equation Solver (EES) from F-Chart Software. The base case assumes a cycle high temperature and pressure of 550K and 30MPa, respectively, a recuperator effectiveness of 92.5% and turbine and compressor efficiencies of 90% and 85%, respectively. Component and piping system pressure drops are based on separate analysis conducted by the authors using the models described below. The base case cycle was optimized at varying compressor suction temperatures to determine the optimal compressor suction pressure and associated thermal efficiency.

Results indicate that the cycle maximum efficiency is very sensitive to the compressor suction temperature. At any given compressor suction temperature, the efficiency has the potential to drop rapidly if compressor suction pressure deviates from a control band. Sensitivity analysis investigates the effects of operating conditions and cycle irreversibilities.

II. Background

Although sCO_2 cycles have been understood to offer significant thermodynamic advantages for decades [1], [2], recent advances in materials and other required technologies have brought this technology to the forefront. The Department of Energy (DOE) summarizes the advantages of sCO_2 as follows [3]:

Energy production, economic and environmental benefits:

- Broad applicability to variety of heat sources
- Higher plant efficiency
- Reduced fuel consumption and emissions
- Low cooling water consumption
- Compact design/footprint lowers capital cost

Public policy benefits:

- U.S. leadership in a transformative technology
- Enhanced U.S. global competitiveness

•Progress towards DOE Strategic Goals and President's Climate Action Plan

Because much of the benefit of sCO_2 as a working fluid (including improved thermal efficiency) arises from its suitability for increased temperature cycles, most of the current research interest (including the DOE's Supercritical Transformational Electric Power or STEP initiative [4]) focuses on elevated temperature applications, generally considered to be greater than 700°C [4]. Nevertheless, even at more moderate temperatures, sCO_2 still offers potentially significant advantages including vastly increased power densities – See Figure 1, which was taken from the DOE's website.

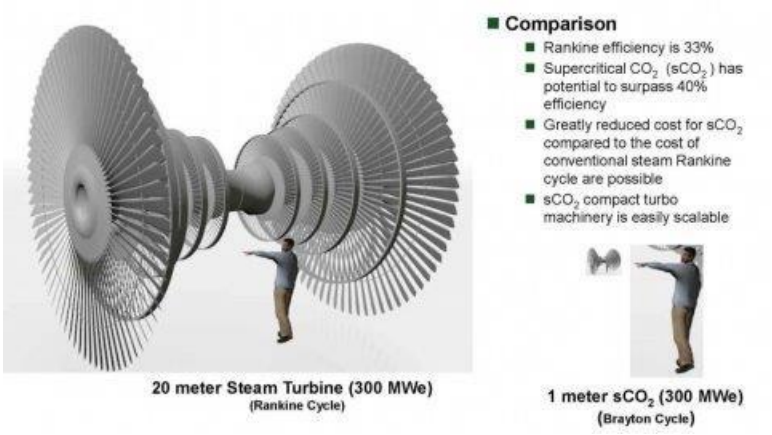

Figure 1. Comparison of Power Densities of sCO_2 and steam cycles [3].

Analysis of sCO_2 cycles, although similar conceptually to other thermodynamic cycles, differs as a result of the unique characteristics of sCO_2. For example, in comparison to air and steam, the pressure ratios are lower by 1 to 5 orders of magnitude. In comparison to steam, the working fluid mass flow rate is about an order of magnitude higher for a similar output power, while the maximum volumetric flow rate is about 3 orders of magnitude lower as a result of the density. For sCO_2 cycles, piping system pressure drops are of a significantly greater concern, and the highly variable specific heat near the critical point requires careful analysis in the regenerative heat exchanger. Maximizing efficiency requires a highly recuperated cycle, but the sensitivity to pressure drops can have adverse effects in enlarged heat exchangers [6]. The highly variable specific heats can create internal pinch points in the recuperator, which can be alleviated with a number of techniques including recompression cycle [5][10] or bypass cycle [13]. On the flip side, because sCO_2 is a single phase working fluid with a high density, it is possible to optimize heat exchangers in a counterflow configuration to greatly enhance heat exchanger effectiveness. Balancing these competing effects requires a robust methodology that optimizes the cycle with consideration of all relevant parameters independently [8].

The present study considered the basic layout, shown in Figure 2b, consisting of a single-shaft compressor and turbine connected to an output electric generator, a compact recuperator and heat supply and heat rejection heat exchangers. To determine sources of irreversibility, the analysis also considered the simple un-recuperated arrangement (Figure 2a), as well as both ideal and real cycles. Inlet and outlet points of each component are defined separately to account for component and piping system pressure drops. Ideal cycles assume an isentropic turbine and compressor and isobaric heat exchangers and connecting piping. The ideal recuperator is assumed to transfer the maximum heat possible in an infinitely large

counterflow configuration $\left(q_{Max}\right)$. The methodology for calculating q_{Max} is discussed below. Real cycles include component pressure drops, pressure drops in connecting piping, turbine and compressor isentropic efficiencies less than unity and heat transfer less than q_{Max} .

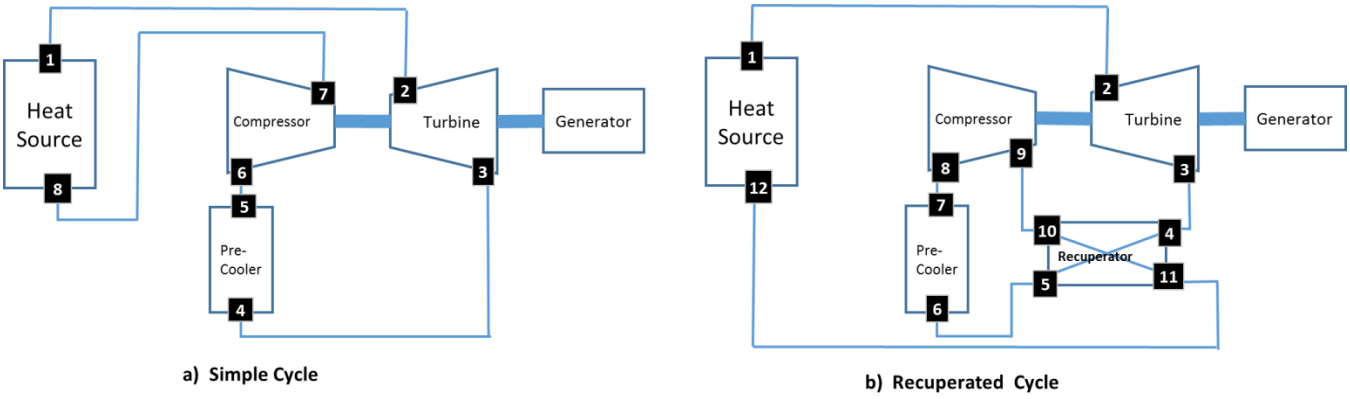

Figure 2—Analysis cycles: a) simple cycle, b) recuperated cycle.

III. Analysis

A. Governing Relationships

For the thermodynamic relationships defined in this section, the subscripts 1 and 2 denote inlet and outlet conditions of the component, respectively. In addition to energy analysis, exergy is used to quantify system losses. Exergy is defined as the useful work that could be extracted by reducing a thermodynamic system to the restricted dead state (T_0 and P_0 represent the local environmental temperature and pressure, respectively). The restricted dead state is appropriate since the system is a non-reacting single substance.

General equations: The energy and entropy balances for a single inlet and single outlet component operating under steady-state conditions are [14],

$$q - w = \left(h_2 - h_1\right) + \left(pe_2 - pe_1\right) + \left(ke_2 - ke_1\right) \quad (1) \quad ; \quad s_{Gen} = s_2 - s_1 - \frac{q}{T} \quad (2)$$

Combining equations (1) and (2) and ignoring the potential and kinetic energy terms yields the exergy (also called availability or available energy) balance [14],

$$\phi_{Heat} - w - i = \psi_2 - \psi_1 \quad (3)$$

where the exergy of the heat source and flow exergy are defined respectively as,

$$\phi_H = q\left(1 - \frac{T_o}{T_H}\right) \quad (4) \quad ; \quad \psi = \left(h - h_o\right) - T_o\left(s - s_o\right) + ke + pe \quad (5)$$

and the irreversibility or exergy destruction is defined in terms of the entropy generation [14],

$$i = T_o s_{Gen} \qquad (6)$$

First law efficiencies and second law efficiencies (sometimes referred to as effectiveness) are defined in terms of energy and exergy balances, respectively [14],

$$\eta_I = \frac{\text{Energy Output}}{\text{Energy Supplied}} \qquad (7) \quad ; \quad \eta_{II} = \frac{\text{Exergy Output}}{\text{Exergy Supplied}} \qquad (8)$$

Heat Source and Heat Rejection Heat Exchangers: The intermediate heat exchanger (IHX) is assumed to receive its heat from a heat source at temperature T_S . For the IHX, energy and exergy balances simplify to,

$$q_S = h_2 - h_1 \quad (9) \quad ; \quad \phi_H - i_{IHX} = \psi_2 - \psi_1 \quad (10)$$

The first and second law efficiencies are,

$$\eta_{IHX,I} = \frac{h_2 - h_1}{q_S} \qquad (11) \quad ; \quad \eta_{IHX,II} = \frac{\psi_2 - \psi_1}{\phi_H} \qquad (12)$$

Because the condenser rejects all of its heat to the environment, all of the exergy removed is destroyed. Thus for the condenser,

$$q_R = h_1 - h_2 \quad (13) \quad ; \quad i_{Cond} = \psi_1 - \psi_2 \qquad (14) \quad ; \quad \eta_{Cond,II} = 0 \qquad (15)$$

Turbomachinery: The energy and exergy balances for the turbine are,

$$w_T = h_1 - h_2 \quad (16) \quad ; \quad w_T = \psi_1 - \psi_2 - i_T \qquad (17)$$

The first law (isentropic) efficiency for the turbine compares actual work that would be realized in a process that exits at the same pressure as the real turbine if the process is isentropic (designated as point 2s). Second law efficiency is the ratio of realized work to exergy supplied.

$$\eta_{T,I} = \frac{h_1 - h_2}{h_1 - h_{2s}} \qquad (18) \quad ; \quad \eta_{T,II} = \frac{h_1 - h_2}{\psi_1 - \psi_2} = 1 - \frac{i_T}{\psi_1 - \psi_2} \qquad (19)$$

The compressor (or pump) governing equations are similarly defined,

$$w_C = h_2 - h_1 \quad (20) \quad ; \quad w_C = \psi_2 - \psi_1 + i \qquad (21)$$

and,

$$\eta_{C,I} = \frac{h_{2s} - h_1}{h_2 - h_1} \qquad (22) \quad ; \quad \eta_{C,II} = \frac{\psi_2 - \psi_1}{h_2 - h_1} = 1 - \frac{i_C}{h_2 - h_1} \qquad (23)$$

Pressure drops and losses to ambient: The system undergoes pressure drops and heat losses to ambient. Head loss in connecting piping is based on the standard equation [16]:

$$\Delta P = \left(\frac{fL}{D} + \sum K \right) \frac{\rho V^2}{2} \qquad (24)$$

where the empirical friction factor f follows the Colebrook-White correlation [15],

$$\frac{1}{\sqrt{f}} = -2Log_{10}\left(\frac{\varepsilon}{3.7D} + \frac{2.51}{Re\sqrt{f}} \right) \qquad (25)$$

The component K values in equation (24) are cataloged from a library of correlations including Crane's Technical Publication Number 410 [12]. Neglecting fouling resistances, which will be very low in sCO_2 systems, heat losses to ambient depend on the internal convection coefficient, pipe wall thermal conductivity, insulation and external convective coefficient [7]. The total heat flow resistance, (defined such that $\dot{Q} = \Delta T / R$) can be determined from the individual resistances,

$$R = \frac{1}{UA} = \frac{1}{hA}\bigg|_{Internal} + \frac{\ln\left(D_o/D_i\right)}{2\pi kL}\bigg|_{Pipe} + \frac{\ln\left(D_o/D_i\right)}{2\pi kL}\bigg|_{Insulation} + \frac{1}{hA}\bigg|_{External} \qquad (26)$$

The internal heat transfer coefficients follow a number of correlations including Dittus-Boelter [7],

$$Nu = \frac{hD}{k} = 0.023 Re^{4/5}\, Pr^{0.3} \qquad (27)$$

Preliminary analysis demonstrated that the internal convective resistance and pipe wall resistance were insignificant in comparison to the external convection and the insulation, so those terms were dropped from the model.

Recuperator: The recuperator is assumed to be adiabatic with respect to the environment. In some applications, such as recompression cycles, mass flow rates of the two streams may differ, but in the present study, the mass flow rate of the hot and cold streams are equal. The resulting energy and exergy balances for the recuperator are,

$$h_{H1} - h_{H2} = h_{C2} - h_{C1} \qquad (28) \quad ; \quad \psi_{H1} - \psi_{H2} = \psi_{C2} - \psi_{C1} + i \qquad (29)$$

where the "C" and "H" subscripts refer to the hot and cold fluids and the "1" and "2" remain inlet and outlet as previously defined. Because the recuperator loses no heat to ambient, it is 100% efficient on a first law basis; the second law efficiency can be determined from,

$$\eta_{\mathrm{Re}cup,II} = \frac{\psi_{C2} - \psi_{C1}}{\psi_{H1} - \psi_{H2}} \qquad (30)$$

Irreversibility occurs in piping and ductwork as a result of pressure drops. Using the full model discussed below, we have determined that heat losses to ambient are small. As a result, for the present problem, piping is assumed to be adiabatic yielding energy and exergy balances of,

$$h_1 = h_2 \qquad (31) \quad ; \quad \psi_1 - \psi_2 = i = T_o\left(s_2 - s_1\right) \qquad (32)$$

In typical applications, the maximum heat transfer possible in a counterflow heat exchanger is proportional to the difference between the inlet temperatures of the two inlet streams [7].

$$q_{Max} = C_{Min}\left(T_{H,i} - T_{C,i}\right) \qquad (33)$$

where C_{Min} is the minimum heat carrying capacity of the two fluid streams :

$$C_{Min} = Min\left(\dot{m}_H\, c_{P,H}, \dot{m}_C\, c_{P,C}\right) \qquad (34)$$

These basic definitions for q_{Max} are applicable in cases of constant specific heats, but they can frequently be used in cases of variable specific heats by assuming an average specific heat [7]. As a result, at q_{Max} the fluid stream with the lower heat capacity exits at the inlet temperature of the other fluid stream. In sCO_2 cycles, however, the great variation in specific heats frequently results in an internal "pinch point," as shown in Figure 3, which limits the maximum heat transfer to a lesser value. To account for the pinch point in the present study, q_{Max} is defined as the amount of heat transfer that would occur in a counterflow heat exchanger of infinite heat transfer area. As Figure 3 shows, when an internal pinch point is present, the maximum possible heat transfer occurs when the temperature profiles of the fluids approach each other. For the profiles shown in the figure, heat transfer at the rate specified in equation (33) would result in a physically impossible situation where the temperature profiles cross each other. The procedure used to calculate q_{Max} is described below.

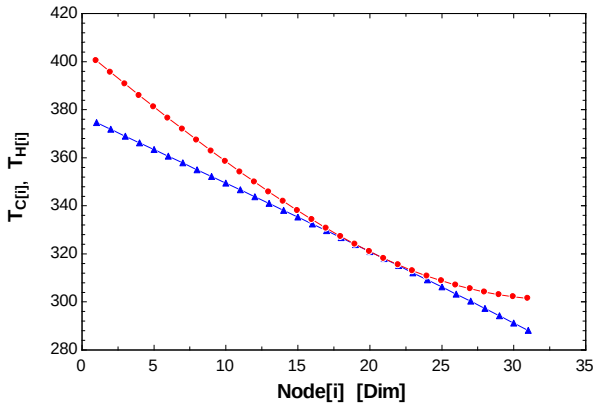

Figure 3. Typical temperature distribution in a counterflow recuperator with the maximum possible heat transfer as limited by an internal pinch point. Representative data for both fluids carbon dioxide with mass flow rates equal, low temperature fluid pressure = 30,000 kPa, high temperature fluid pressure = 6940kPa, high temperature fluid inlet temperature = 400K, low temperature fluid inlet temperature = 288K.

Heat exchanger effectiveness is defined as the heat transfer normalized by the maximum possible heat transfer [7],

$$\varepsilon = \frac{q}{q_{Max}} \qquad (35)$$

The thermal efficiency of the plant considers only the secondary cycle shown in Figure 2 ,

$$\eta_{th} = \frac{w_{NET}}{q_S} = 1 - \frac{q_R}{q_S} \quad (36)$$

B. Computational Methods

The analysis equations summarized above were programmed using Engineering Equation Solver (EES) from F-Chart Software®. The completed model, which contains about 400 equations, was written to analyze the secondary sCO_2 plant along with an associated pressurized water reactor (PWR) as its heat source and tertiary heat sink cooling system as shown in Figure 4. The bypasses, "FM3" and "FM4", allow flow through their associated throttle valves are inserted for controllability of the system. The recuperator is segmented into 30 sections to determine the internal pinch point and the IHX is segmented into 10 sections. Each motor and generator efficiency is selectable. Pressure drops are determined from pipe flow correlations, including the tees, which depend on flow splits. The motor on the compressor shaft can be modeled as a prime mover for the compressor, or reversed and used as a generator.

The model allows for a number of simplified calculations that are used to initialize parametric guess values, which are critical in obtaining convergence to a solution when using EES. After initial guess values are determined, the full analysis can be run.

For the results summarized in section IV.A, IV.B and IV.C, below, the mass flows "FM3" and "FM4" were set to zero. In addition the efficiency of the compressor turbine and main turbine were both set to 90% and the associated pressure drops from point 1 to points 2 and 13 are equal as listed below. The full model has been run to establish realistic piping system pressure drops and heat losses. These results are incorporated into the input values. Results using all of the computational abilities of the full model in Figure 4 will be presented in the future.

The model includes two recuperator calculation options. The first option allows a fixed heat transfer capacity (UA) to be inserted to determine the projected heat transfer. The effectiveness is an output based on the inserted UA. The second option allows the effectiveness to be an input variable and the required UA as an output. The recuperator q_{Max} is determined using an EES procedure, which divides the recuperator into segments of equal heat transfer. The rate of heat transfer is iterated to determine the heat transfer rate necessary to have the temperatures of the two fluid streams equal at a given internal location. It was determined that 30 segments were sufficient to reduce error to less than 0.01% in test cases.

The internal EES library was used for property values, with the reference point set at the Institute of Refrigeration (IIR) reference state. For validation purposes, values from the EES library were compared against NIST Standard Reference Database 23: Reference Fluid Thermodynamic and Transport Properties-REFPROP, Version 9.1, National Institute of Standards and Technology, Standard Reference Data Program, Gaithersburg, 2013. In most cases, EES library values were within 0.003% of REFPROP values. Near the critical point errors approached 1% in enthalpy and 0.8% in entropy. (Values for thermal conductivity and viscosity approached 15% and 20% respectively at the critical point, although these values were not used in the current model.)

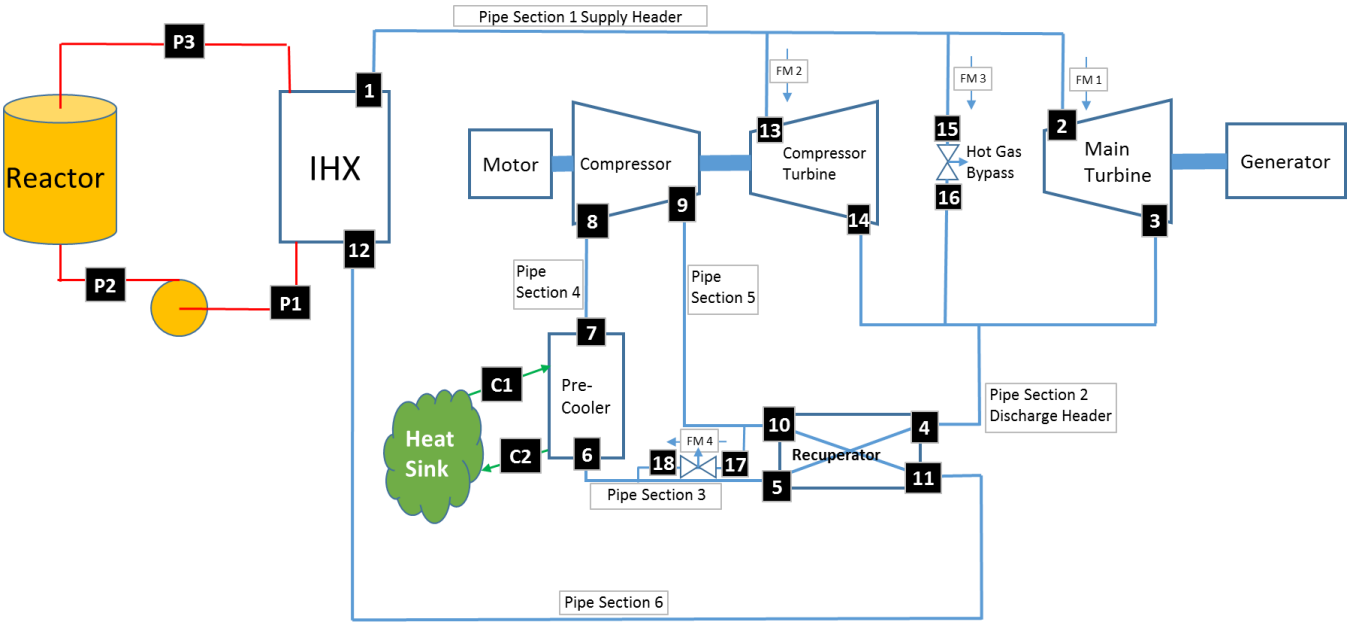

Figure 4. Plant configuration used in the system model. A small modular nuclear reactor (SMR) operates in a pressureized water reactor configuration supplying heat to a secondary sCO_2 cycle. The compressor, compressor turbine and main turbine have independely controllable "turbomachinery maps." The bypasses, "FM3" and FM4", that allow flow through associated throttle valves are inserted for controllability of the system. The recuperator is segmented into 30 sections to determine the internal pinch point and the IHX is segmented into 10 sections. Each motor and generator efficiency is selectable. Pressure drops are determined from pipe flow correlations, including the tees, which depend on flow splits. The motor on the compressor shaft can be modeled as a prime mover for the compressor or reversed and used as a generator.

IV. Results and Analysis

The present study is focused primarily on sCO_2 cycles receiving heat from a pressurized water nuclear reactor operating at moderate operational temperatures. Operational conditions at the exit of the heat source were selected as T-high = 550K and P-high = 30MPa. Cycle low temperatures, $T^* = T/T_{Crit}$, were varied from 0.9 to 1.1 (T^* = 0.9, 0.95, 0.98, 1.0, 1.02, 1.05, 1.1) to determine the optimal low pressure.

The results are organized as follows: In subsection A), the recuperated and un-recuperated ideal cycles are briefly considered. For each of the cycle low temperatures, the cycle low pressure is varied to optimize the thermal efficiency. In subsection B), real cycles with expected irreversibilities are considered. The results are analyzed to determine ideal operating pressure and efficiency as a function of cycle low temperature and associated sources of cycle irreversibility. Finally subsection C) contains a parametric analysis of the real recuperated cycle to determine the effects of varying the operating parameters, including cycle high temperature, cycle high pressure, pressure drops, component efficiencies and recuperator effectiveness.

A. Ideal Cycle

The thermal efficiencies for the simple and recuperated ideal cycles summarized in Table 1 are shown in Figure 5. Recuperated cycle efficiency decreases to less than the un-recuperated cycle at the point the recuperator transfers heat in the reverse direction. At subcritical temperatures (shown in the T* = 0.95 case), this corresponds to pressures less than the saturation pressure, and the transition is marked by a rapid (step change) loss of efficiency. At supercritical temperatures, the efficiency curve is smooth. For

T_{Low} at the critical pressure, the real recuperated has an inflection point on the efficiency curve at the critical pressure.

The high thermal efficiencies shown on Figure 5 for the un-recuperated cycle (increasing as cycle low pressure decreases) have no practical value in actual applications. Here, the cycle behaves as a simple Brayton cycle with a high back work ratio (compressor work is a large fraction of turbine work). As shown below, with realistic turbomachinery efficiencies, the cycle efficiency drops similarly to the recuperated cycle and continues to decline. The ideal cycles also show increasing efficiency as the low side pressure continues to increase. This too is of no practical value. Here, as the pressure ratio approaches unity, pinch point losses in the recuperator are decreased, increasing the amount of heat recuperated. However, as shown below, component pressure drops cause the efficiency to decrease from a maximum as the low side pressure is further decreased.

Table 1. Cycle operating conditions for simple and recuperated ideal cycles. Piping system and component pressure drops based on concept design studies. Component efficiencies are based on literature survey.

	Simple Cycle (Figure 2a)	Recuperated Cycle (Figure 2b)
Point 1 Properties Temperature (K) Pressure (MPa)	550 30	
Efficiency Turbine Compressor	Isentropic Isentropic	
Recuperator Effectiveness		100%
Piping and component pressure drops	Isobaric	

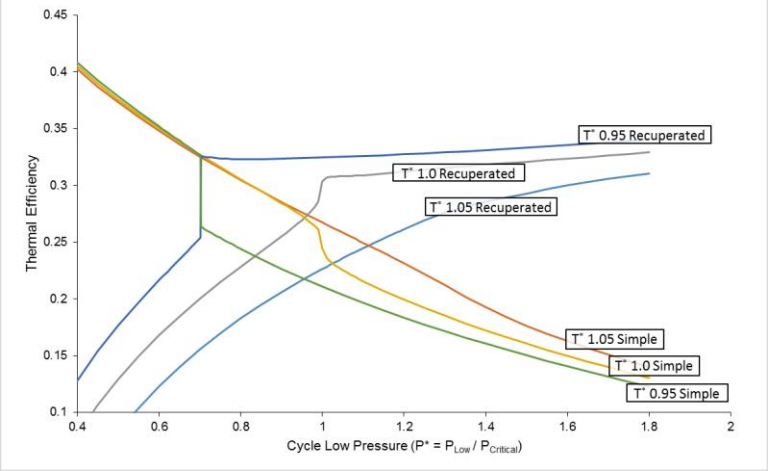

Figure 5. Ideal efficiencies for simple and recuperated cycles. Recuperated efficiencies drop to less than simple cycles for cases when recuperator heat transfer is in the reverse direction.

B. Real Cycle

Operating conditions and component losses for the real simple cycle (Figure 2a) and the real recuperated cycle (Figure 2 b) are summarized in Table 2. Piping system pressure drops are based on the results of several concept plant designs performed at Newport News Shipbuilding using the full system shown in Figure 4. Component efficiencies are consistent with currently accepted values in the scientific literature.

Table 2. Cycle operating conditions for simple and recuperated real cycles. Piping system and component pressure drops are based on concept design studies. Component efficiencies are based on literature survey.

	Simple Cycle (Figure 2a)	Recuperated Cycle (Figure 2b)
Point 1 Properties		
Temperature (K)	550	
Pressure (MPa)	30	
Efficiency		
Turbine	90%	
Compressor	85%	
Recuperator Effectiveness	--	92.5%
Component pressure drops (kPa)		
Pre-cooler	100	100
IHX	150	150
Recuperator (cold)	--	30
Recuperator (hot)	--	50
Piping pressure drops (kPa)		
Section 1-2	80	80
3-4	10	10
5-6	40	5
7-8	200	40
9-10	--	35
11-12	--	200

In contrast with the ideal cycle summarized above, the real cycle has a distinct maximum in thermal efficiency in all cases shown in Figure 6. There is a small range where the un-recuperated cycle is more efficient than the recuperated if pressure is allowed to drop below its optimum operating pressure; however, at the level, the system is operating well outside of its desired operating band.

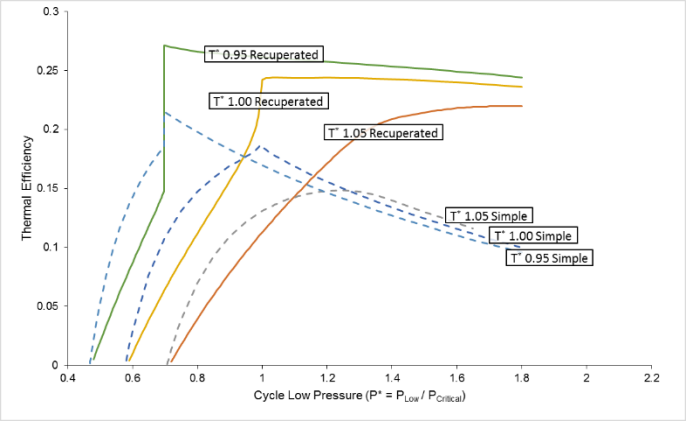

Figure 6. Efficiencies for simple and recuperated real cycles, assuming the operating conditions listed in Table 2. Recuperated efficiencies drop to less than simple cycles for cases that recuperator heat transfer is in the reverse direction. Real and ideal efficiencies are also equal when net cycle work decreases to zero.

Figure 7 shows a plot of the thermal efficiency as a function of cycle low pressure for various cycle low temperatures. As the plot shows, for subcritical temperatures, the efficiency undergoes a steep drop if pressure decreases below a critical value. With a low cycle temperature equal to the critical temperature, the efficiency curve still has a distinctive steep reduction, although it does not have the vertical step change. As temperature is further increased, the efficiency curves lose the distinct drop in efficiency, although they maintain a maximum efficiency value.

Figure 8 shows the maximum thermal efficiency (right scale) and corresponding compressor suction pressure (left scale) for the cycle identified in Table 2 as a function of compressor suction temperature. The figure also shows saturation conditions and pressures for thermal efficiencies equaling 98% of the maximum. (The two 98% data sets correspond to pressures above and below the optimum thermal efficiency.) At compressor suction temperatures below the critical temperature, cycle thermal efficiency is maximized when compressor suction pressure equals saturation pressure. Efficiency drops dramatically if pressure is decreased below saturation. Under these subcritical conditions, the low side 98% data is coincident with the maximum efficiency as a result of the step reduction in efficiency at saturation and efficiency drops smoothly as pressure increase above saturation. As temperature approaches saturation, maximum efficiency and 98% curves diverge as a result of the behavior noted in Figure 7.

The reasonable operating curve balances efficiency, margin to adverse operating conditions and piping stresses. Under subcritical temperatures, the operating curve provides some margin to the sharp reduction noted at saturation but maintains efficiency greater than 98% of the maximum. As temperature surpasses the critical temperature, the curve allows pressures less than the maximum efficiency to limit the stress requirements on the low pressure side.

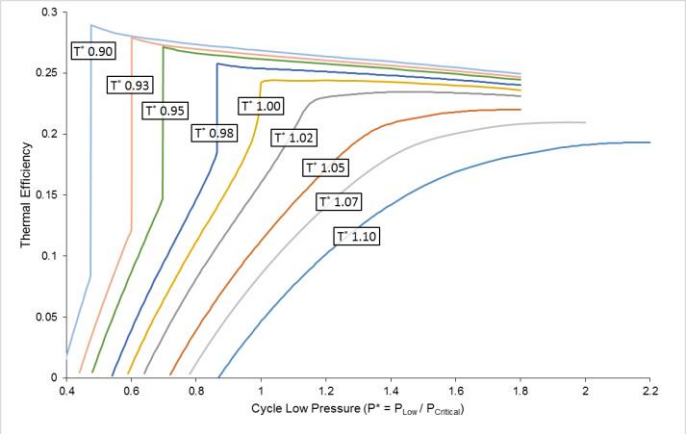

Figure 7. Thermal efficiencies for recuperated cycle specified in Table 2. Each curve represents the thermal efficiency at a specified cycle low temperature as a function of cycle low pressure.

For illustrative purposes, the energy and exergy balances of a small modular reactor (SMR) configured as a pressurized water reactor supplying heat to an sCO_2 cycle are tabulated in Table 3. The reactor analyzed is a nominal 100MW reactor operating with an average temperature of 540K. As the exergy balance reveals, the greatest sources of exergy destruction in the cycle are the temperature drops in the reactor and the IHX. The secondary plant has second law efficiency of 68%. The greatest source of exergy destruction in the secondary plant is heat rejection to the pre-cooler, although recovery of the rejected exergy would be difficult, based on the relatively low temperature. Turbine, compressor and recuperator losses are all relatively small (5-8% of the supplied exergy). The figures in this table depend on the assumed temperatures for the heat source and the environment and are only intended to provide relative magnitudes.

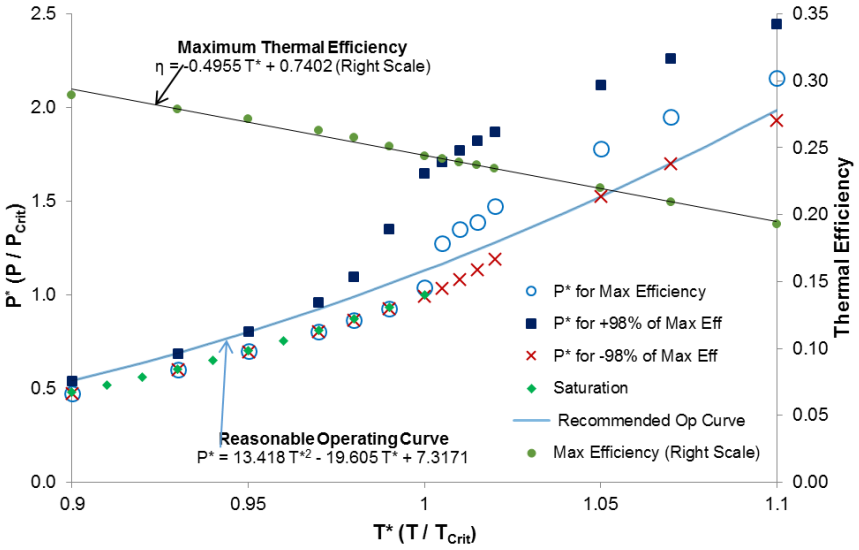

Figure 8. Critical low side operating pressure and thermal efficiency (Right Scale) for the cycle specified in Table 2 as a function of T^*_{Low}. The reasonable operating pressure curve results in a thermal efficiency of 98% of the maximum possible. For cycle low temperatures less than the critical temperature ($T^*_{Low} < 1.0$), pressure is maintained at a value greater than that of the optimum efficiency to reduce the chance of the sharp reduction noted in Figure 7. For T* > 1, the pressures are less than the pressure for optimal efficiency to reduce pipe stresses.

Table 3. Energy and exergy balances of a hypothetical Small Modular Reactor (SMR) pressurized water reactor plant coupled with an sCO_2 secondary plant operating at the conditions specified in Table 2 with T^*_{Low}=1.0 and P_{Low}* = 1.13. Exergy values are based on a maximum heat source temperature of 1100K and a dead state temperature of 298K. Primary loop average temperature is 540K.

	Energy Balance (MW in)	Exergy Balance (MW in)
Primary Loop		
Supplied by Fission	100.00	72.91
Reactor Losses	0.00	-28.18
Primary Coolant Pump	0.23	0.23
Supplied to IHX	-100.20	-44.96
IHX		
Supplied from Primary	100.20	44.96
Loss	0.00	-9.24
Supplied to sCO_2	-100.20	-35.72
sCO_2 Loop		
Supplied from IHX	100.20	35.72
Compressor Work	13.65	13.65
Turbine Work	-38.08	-38.08
Piping Losses	0.00	-0.24
Turbine Losses	0.00	-2.96
Compressor Losses	0.00	-1.82
Recuperator	0.00	-1.83
Pre-cooler	-75.80	--4.44

C. Parametric Analysis

A parametric analysis considered the effects of varying operating parameters on three separate base cases. The three base cases include a subcritical low temperature, (T*=0.95), low temperature at the critical point and a supercritical low temperature, (T*=1.05).

The parametric analyses considered are summarized in Table 4. In each case, only the indicated parameters were varied from the base case. In cases 1, 2 and 4, only the single parameter was varied. In cases 3 and 5, each of the components was varied simultaneously, in a proportional manner. For example, in case 3, compressor efficiency of 70% corresponded to a turbine efficiency of 80% and compressor efficiency of 92.5% corresponded to a turbine efficiency of 95%. In case 5, the ratio of pressure drops is constant.

Table 4. Parametric sensitivity analysis. In the analysis, only the indicated parameters were varied from the base case. In cases 1, 2 and 4, only the single parameter was varied. In cases 3 and 5, each of the components was varied simultaneously, maintaining a constant loss ratio of each. For example, in case 3, the compressor losses are always 150% of the turbine losses (a turbine efficiency of 80% is matched with a compressor efficiency of 70%).

		Sensitivity Analysis Cases				
	Base Case	1 T_H (T_1)	2 P_H (T_9)	3 Component Efficiency	4 Recuperator Effectiveness	5 Pressure Drops
Point 1 Temperature (K)	550	450 - 700				
Point 1 Pressure (MPa)	30		25 - 40			
Efficiency						
Turbine	90%			80% - 95%		
Compressor	85%			70% - 92.5%		
Recuperator Effectiveness	92.5%				85% - 100%	
Component pressure drops (kPa)						
Pre-cooler	100					50-200
IHX	150					75-300
Recuperator (cold)	30					15-60
Recuperator (hot)	50					25-100
Piping pressure drops (kPa)	---	-------	-------	-------	-------	----
Section 1-2	80					40-160
3-4	10					5-20
5-6	5					2.5-10
7-8	40					20-80
9-10	35					17.5-70
11-12	200					100-400

As expected Figure 9 shows that the thermal efficiency is highly dependent on the cycle high temperature (T_1) as well as cycle low temperature (T_7). In order to limit the variation to a single parameter, the three curves shown in the figure use a cycle low pressure that optimizes the thermal efficiency when T_1 = 550K. A separate optimization demonstrated that efficiency could be improved by simultaneously varying cycle low pressure as T_1 is varied, but the maximum improvement observed was 0.19%. The curves shown are smooth and follow the same general shape as the Carnot efficiency. However, at low cycle temperature, the real cycle values achieve a lower fraction of the Carnot efficiency than they do at higher temperatures. For example, at 450K real cycles are about 41% to 47% of their respective Carnot efficiencies, while at 700K the values range from 57% to 61%. The divergence from Carnot also increases as cycle low temperature increases.

Figure 10 shows the effect of system pressure drops. The overall behavior of the curves remains unchanged and as expected, increasing pressure drops lower thermal efficiency. The insert amplifies the effect in the parametric range of interest.

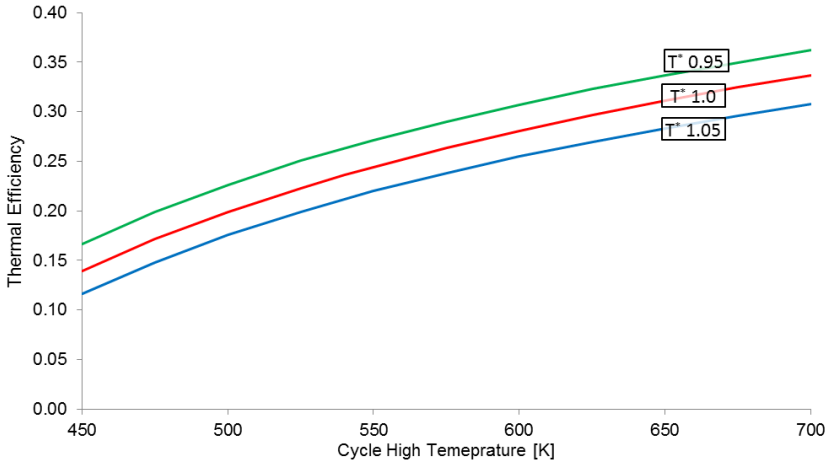

Figure 9. Effect of cycle high temperature on cycle efficiency.

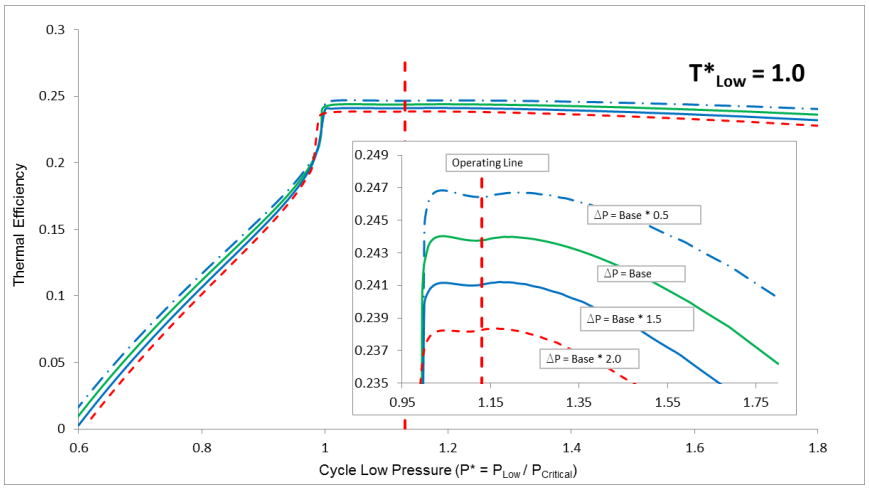

Figure 10. Effect of pressure drops on cycle efficiency. The series of curves represent base case pressure drops multiplied by a factor ranging from 0.5 to 2.0.

In Figure 11, plant thermal efficiency is significantly degraded by turbomachinery performance. In this analysis, the turbine and compressor were degraded together in a manner that the divergence from isentropic was consistent. Specifically, the base case is $\eta_T = 0.9$ and $\eta_C = 0.85$. When the turbine efficiency was lowered to $\eta_T = 0.8$ compressor efficiency was lowered to $\eta_C = 0.70$, and when turbine efficiency was raised to $\eta_T = 0.95$ compressor efficiency was raised to $\eta_C = 0.925$. Figure 11A shows the effect on thermal efficiency. Figure 11B shows the corresponding component irreversibilities.

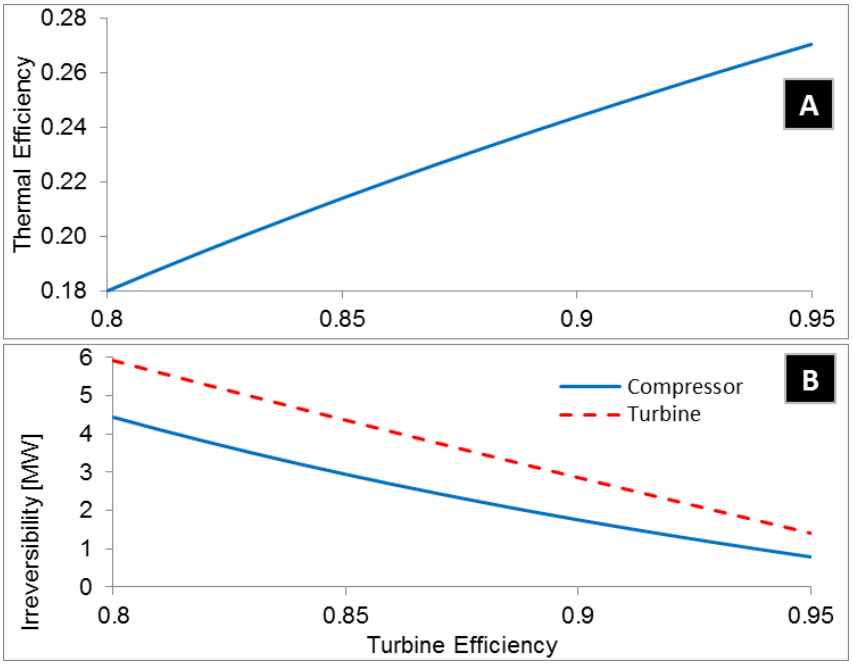

Figure 11. Effect of Turbomachinery efficiency on system behavior. The compressor efficiency is varied such that difference from 100% is always 150% of that of the turbine. A) Plant Efficiency and B) Component and Turbine Irreversibility

Figure 12 details the effect of recuperator effectiveness. As subfigure A demonstrates, the required heat exchanger area increases as the desired effectiveness increases. The main part of this figure is roughly linear on a logarithmic plot (exponential), but then tapers as unity is approached. The insert, plotted on a linear plot shows that at around 98% effectiveness, the required area increases greatly. The corresponding efficiency is shown in subfigure B. The recuperator, overall, raises the efficiency from about 16% to 26% (a 63% improvement). However combining the results of subfigures A and B, the marginal gain in efficiency diminishes as the area increases. In this study, we used a 92.5% effective recuperator as a base case, which provides a great efficiency enhancement, but avoids the steep part of the increased area shown in sub figure A. Sub figure D shows that the recuperator irreversibility increases as area increases, since the level of heat transfer increases until it reaches a point where the decreased temperature difference overrides the heat transfer effect. Even where the recuperator irreversibility increases, the total irreversibility decreases because recuperation decreases irreversibility in the IHX and pre-cooler. The analysis here did not add a penalty for increase pressure drop as area increases. (Pressure drops were held constant.) Had pressure drops been increased, the thermal efficiency curve would have achieve a maximum and then started to decrease at an effectiveness that is close to unity.

The effect of cycle high pressure is shown in Figure 13. In each of the cases shown (T^*_{Low} ranging from 0.95 to 1.05), the efficiency is greatest at the 30 MPa in the region near the desired operating conditions, although the variation is not strong. Operating between 25 MPa and 30 MPa allows a relatively wide operational band and reasonable piping stresses. As the figures show, increasing to 35MPa and even 40 MPa is detrimental on efficiency and also increases piping stresses.

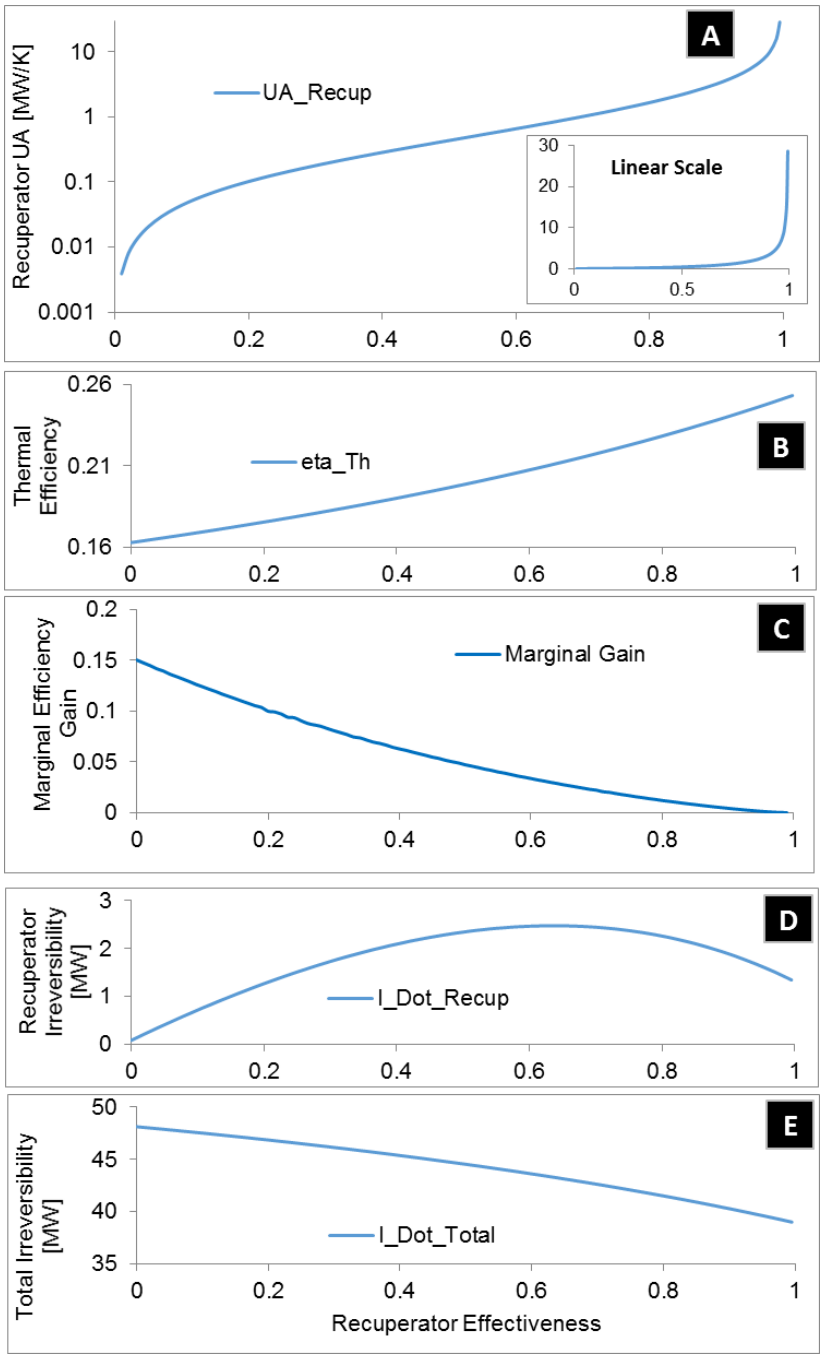

Figure 12 Effect of Recuperator Effectiveness. A) The recuperator area (represented as UA in MW/K) required for the designated effectiveness B) Cycle efficiency for the given effectiveness, C) Marginal gain in efficiency ($\Delta\eta/\Delta$UA) as a function of effectiveness. As the curve demonstrates, increasing UA has a diminishing return on investment. D) Recuperator irreversibility and E) Total cycle irreversibility.

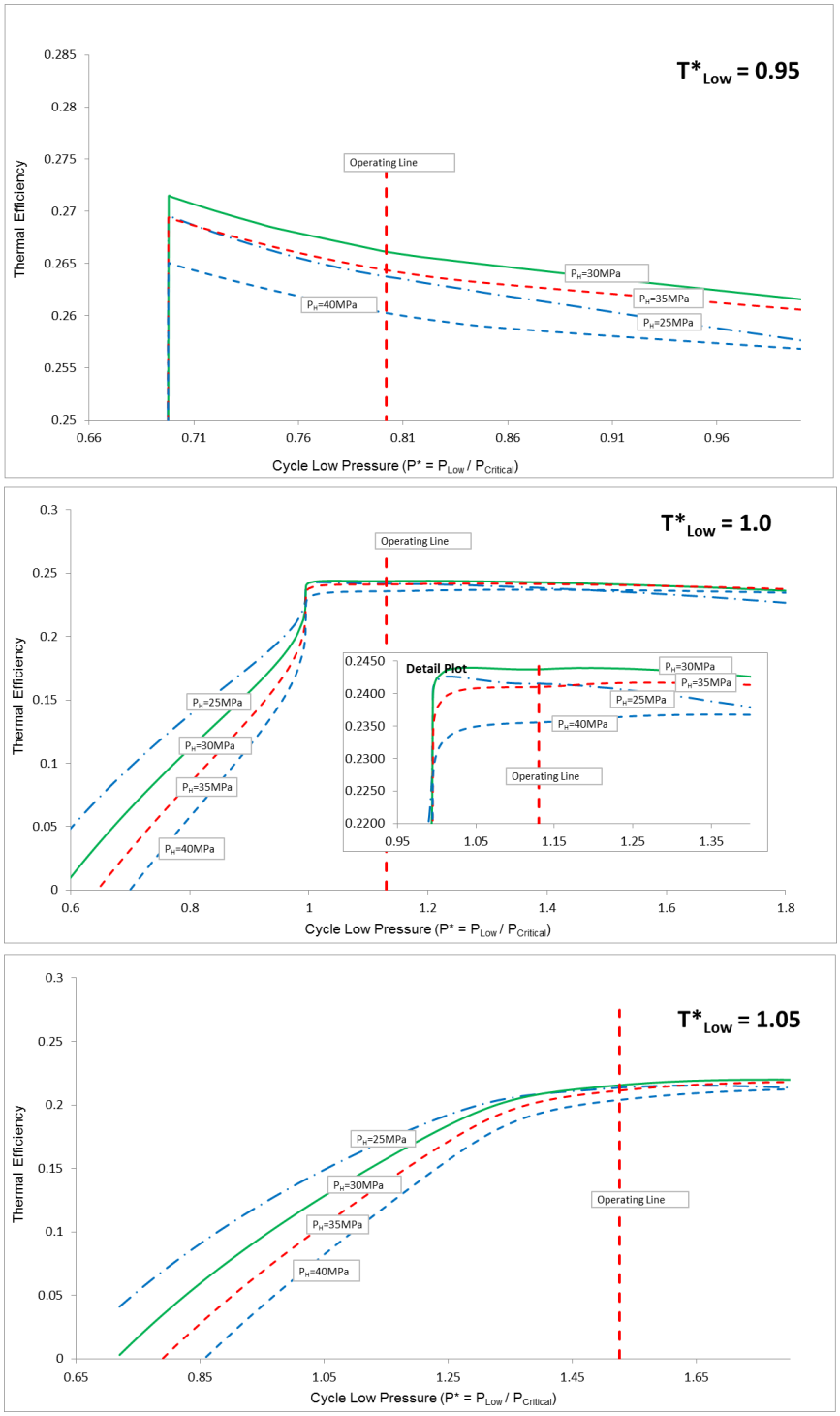

Figure 13. Effect of cycle high pressure on thermal efficiency. Selected curves from Figure 7 are re-plotted here along with additional curves at differing cycle high pressures.

V. Conclusions

In this paper, we have investigated the thermal efficiencies and losses in simple and recuperated sCO_2 power cycles operating at moderate peak cycle temperatures (450K to 700K). The following conclusions are supported by the data summarized above:

1. For a given cycle high temperature and pressure, ideal recuperated cycles (isentropic turbomachinery, ideal recuperation and isobaric heat exchangers) have a thermal efficiency that continues to increase as the cycle low pressure is increased. This relationship results from the elimination of the recuperator pinch point as the cycle high and low pressures approach each other. Un-recuperated ideal cycles have thermal efficiencies that increase as the cycle low pressure is decreased. These ideal cycles have little practical value since in real cycles the trends are reversed as a result of irreversibilities.
2. Over the parametric range tested, the thermal efficiency of real recuperated cycles is strongly dependent on the cycle high and low temperatures.
    a. Efficiency of the cycle increases as the compressor suction temperature is decreased.
    b. The efficiency increases smoothly as turbine inlet temperature increases. The increase shows that the efficiency roughly doubles as the turbine inlet temperature increases from 450K to 700K.
3. Thermal efficiency is strongly dependent on cycle low pressure.
    a. For subcritical cycle low temperatures, maximum efficiency occurs when the cycle low pressure equals the saturation pressure. Efficiency drops in a step change if the pressure drops below the saturation pressure as a result of greatly increased pumping losses along with recuperator heat transfer going in the reverse direction. Efficiency drops gradually and smoothly if cycle low pressure is increased above saturation pressure.
    b. For cycles operating above the critical temperature, efficiency decreases smoothly and gradually if pressure deviates from the ideal.
    c. A suitable suction low pressure provides a reasonable safety margin with less than a 2% reduction in efficiency. The recommended curve achieves 98% of the maximum efficiency at subcritical temperatures (by maintaining pressure slightly above saturation) and limits mechanical stresses at supercritical temperatures (by operating at pressures below the maximum efficiency).
4. Cycle irreversibilities reduce the thermal efficiency as expected.
    a. System pressure drops over the range of parameters tested have a relatively small influence on cycle efficiency.
    b. Because of the magnitude of the back work, turbomachinery efficiencies have a large influence on cycle efficiencies.
5. Increasing recuperator area increases efficiency but at a diminishing rate as area increases.

References

[1] Angelino G., “Carbon Dioxide Condensation Cycles for Power Production”, ASME Paper No. 68-GT-23, (1968).
[2] Angelino G., “Real Gas Effects in Carbon Dioxide Cycles”, ASME Paper No. 69-GT- 103, (1969).
[3] Department of Energy sCO_2 Team. http://energy.gov/supercritical-co2-tech-team

[4] DOE solicitation DE-SOL-0007963 https://www.fedconnect.net/fedconnect/?doc=DE-SOL-0007963&agency=DOE

[5] Dostal,Y ; Driscoll,M.J. and Hejzlar, P., "A Supercritical Carbon Dioxide Cycle for Next Generation Nuclear Reactors," Available at: http://web.mit.edu/course/22/22.33/www/dostal.pdf

[6] Fourspring, Patrick and Nehrbauer, Joseph, "Heat Exchanger Testing for Closed Brayton Cycles Using Supercritical CO2 as the Working Fluid," The 3rd International Symposium - Supercritical CO2 Power Cycles May 24-25, 2011, Boulder, Colorado. Available at: https://drive.google.com/file/d/19JUuH6BiVmE4zvBAtksYco02FNroMdQlqcUigkrVEpAAq9oijOFsDJoYWn7A/view?pli=1

[7] Incropera, Frank P and Dewitt, David P., *Introduction to Heat Transfer, 4th Ed*, John Wiley and Sons, 2002.

[8] Mohagheghi, Mahmood and Kapat, Jayanta, "Thermodynamic Optimization of Recuperated s-CO2 Brayton Cycles for Waste Heat Recovery Applications," The 4th International Symposium - Supercritical CO2 Power Cycles September 9-10, 2014, Pittsburgh, Pennsylvania. Available at: http://www.swri.org/4org/d18/sCO2/papers2014/systemModelingControl/43-Mohagheghi.pdf

[9] Morosuk, Tatiana and Tsatsaronis, George, ADVANCED EXERGETIC ANALYSIS AS A TOOL FOR THE THERMODYNAMIC EVALUATION OF SUPERCRITICAL CO2 POWER CYCLES, The 4th International Symposium - Supercritical CO2 Power Cycles September 9-10, 2014, Pittsburgh, Pennsylvania. Available at: http://www.swri.org/4org/d18/sCO2/papers2014/systemModelingControl/49-Tsatsaronis.pdf

[10] Sarkar, Jahar, "Second law analysis of supercritical CO2 recompression Brayton cycle," Energy, Vol 34, Sep 2009, pp. 1172-1178.

[11] Sulzer, G., Verfahren zur Erzeugung von Arbeit aus Warme, Swiss Patent CH 269-599, 1950.

[12]Technical Publication Number 410, Crane Company, Joliet, IL, 1991.

[13]Vaclav, Dostal and Jan, Dostal, "Supercritical CO2 Regeneration Bypass Cycle – Comparison to Traditional Layouts," The 3rd International Symposium - Supercritical CO2 Power Cycles May 24-25, 2011, Boulder, Colorado. Available at: https://drive.google.com/file/d/1Ga_q6P_vOmORidiRtJNM-YrhrRXgAQP86ze5srVR43_yKa33iyRzkhNMiQQ2/view?pli=1.

[14] Wark, Kenneth M., Advanced Thermodynamics for Engineers, McGraw-Hill, Inc., 1995.

[15] White, Frank M., Hess, John L., and Gibson, Carl H., "Equations of Fluid Static and Dynamics," *Fundamentals of Fluid Mechanics,* Schetz, Joseph and Fuhs, Allen E. (Eds), John Wiley and Sons, 1999

[16] Young, Donald F., Munson, Bruce R., and Okiishi, Theodore, H., *Brief Introduction to Fluid Mechanics*, John, Wiley and Sons, 1997.